Toward magnetic field dissipation during the 23 July 2002 solar flare measured with Solar and Heliospheric Observatory/Michelson Doppler Imager (SOHO/MDI) and Reuven Ramaty High Energy Solar Spectroscopic Imager (RHESSI)

Valentina V. Zharkova, Sergey I. Zharkov, Stanley S. Ipson, and Ali K. Benkhalil

Department of Cybernetics and Virtual Systems, University of Bradford, Bradford, UK

[1] We analyze the SOHO/MDI high-cadence magnetic field variations that occurred in a bipolar area around the apparent neutral line (ANL) prior to and during the $2B/X4.8$ flare on 23 July 2002 and their association with the hard X-ray (HXR) and H_α emission observed with RHESSI and BBSO. Magnetic field changes started 6 min prior to the hard X-ray emission onset in $0.3-2$ MeV band or 7 min in the $12-25$ keV band and finished 20 min later. Before the flare, there are nine preexisting sources of a strong magnetic field of the positive and negative polarities, and six new magnetic sources associated with the hard X-ray foot points emerged 2 min before the flare maximum: two negative and four positive ones. The difference magnetograms show a steady movement with a speed of 250 km/s of the magnetic field changes toward the northeast, or a 'negative magnetic field discharge' associated with the magnetic energy release in this flare. The magnetic field changes in the whole flaring area are irreversible, showing an increase of the magnetic flux from 6.7×10^{21} Mx up to 7.9×10^{21} Mx lasting for 6 min and returning after to noise fluctuations about the new magnitude. There is an irreversible increase by -120 G of an absolute magnitude of the negative magnetic field component. The rate of magnetic field changes deduced from the total area around the ANL and from the areas of the hard X-ray foot point with the irreversible changes is about 3.1×10^{18} Mx/s, and the average Poynting flux is $(5-20) \times 10^{11}$ erg/cm^2/s. The LOS fraction of a magnetic energy released for the whole flare duration is estimated as $\sim(2.3-10) \times 10^{31}$ erg. The possible scenarios of particle acceleration in this flare are proposed based on HXR and γ-ray emission.

1. Introduction

[2] It is widely accepted that the source of primary energy release in solar flares is associated with magnetic energy dissipation via a reconnection of magnetic lines in the corona while the released energy is transported into deeper atmospheric levels by fast particle beams, heating fluxes or waves [*Moore et al.*, 1984; *Somov*, 2000; *Priest and Forbes*, 2000]. The mechanisms of energy release and transport in solar flares are not fully understood, mainly because of incomplete knowledge of the magnetic field changes that occur in flares. There are no means yet to observe directly the magnetic field variations in the corona but only infer them from the measurements in the photosphere and chromosphere.

[3] In the past two decades there were a few attempts to measure the magnetic field changes associated with flares. Strong impulsive magnetic field changes, or magnetic transients, were detected in solar flares a long time ago with a light-of-sight (LOS) videomagnetograph [*Patterson and Zirin*, 1981; *Zirin and Tanaka*, 1981]. However, the interpretation of these observations led to the conclusions that the observed variations were caused by an increase of spectral line emission during flares [*Patterson*, 1984]. Recently, fast magnetic field variations were detected for the Bastille flare 2000 [*Kosovichev and Zharkova*, 2001] using the LOS SOHO/MDI observations for the flare located at the center of a solar disk (the LOS component is a vertical one). The magnetic field changes in this flare

were of the two types: irreversible ones with the LOS component of magnetic field permanently decreased prior and during the flare by a significant value of a few hundred Gauss and reversible ones with the magnetic field decreasing during the flare and returning back to the preflare level after it. The former were attributed to a process of magnetic energy dissipation and the latter to the transport processes of accelerated particles meaning the Ni atom excitation by fast nonthermal electrons that leads to an increase of the Ni 6768A intensity and a change of its line profile [*Zharkova and Kosovichev*, 2002]. However, these changes were found not to last longer than a minute and do not affect the line profile after this time.

[4] Apart from a few cases above there are no systematic observations with high-temporal resolution of the magnetic energy dissipation in solar flares. Mostly this is because of the first unsuccessful attempts [*Patterson and Zirin*, 1981] and the following criticism of any LOS magnetic observation that were expected to be caused by the line intensity variations. Later the magnetic variation were separated into the two classes: reversible and irreversible [*Kosovichev and Zharkova*, 2001], this gave another boost to the investigation of fast magnetic variations associated with flares. Taking into account that the reconnecting magnetic loops are embedded into the photosphere and expand into the corona according to the global reconnection models, from the observations of LOS fast magnetic field variations in the photosphere associated with a preflare phase, flare onset and its gradual phase, one can extrapolate the magnetic variations into higher atmospheric levels and estimate the visible magnetic reconnection rate and energy released in a solar flare.

[5] Some observers reported a decrease in the magnetic field strength after flares [*Moore et al.*, 1984; *Kosovichev and Zharkova*, 2001], in the observations of the near-limb flare magnetic field weakened in one (vertical) polarity while strengthened in the other (horizontal) one [*Cameron and Sammis*, 1999]. From the theoretical modeling and some limited observations of the full magnetic vector in the vicinity of strong flares the magnetic changes were found to occur near the magnetic field location with a strong gradient across the apparent neutral line of the vertical component while the horizontal component has a strong shear [*Priest and Forbes*, 2000; *Somov*, 2000]. Although the shear is expected to decrease during the course of a flare, when the magnetic field dissipates, the observations reveal that in some cases the shear still increases [*Wang et al.*, 1994, 2002].

[6] The investigation of coronal magnetic fields extrapolated from the photospheric LOS magnetograms reveals a consistent spatial and temporal correlation between the locations of energy release in solar flares and the regions of strong variations of the field line connectivity [*Mandrini et al.*, 1995; *Demoulin et al.*, 1997]. These regions called quasi-separatrix layers (QSLs) are considered to be a signature of magnetic reconnection in solar flares [*Longcope and Strauss*, 1994; *Priest and Demoulin*, 1995]. Analyzing the mapping produced by LOS magnetic field lines on the photosphere, a detailed description of the magnetic line connectivity in these QSLs was introduced [*Titov et al.*, 1999; *Titov and Hornig*, 2002] based on the global reconnection models [*Gorbachev and Somov*, 1988; *Somov*, 2000].

[7] The coronal magnetic field line mapping from the LOS photospheric measurements based on a force-free interpolation [*Titov et al.*, 1999, 2002] has shown the locations of separatrices in the two loops reconnecting in the corona and the position of a separator for these loops with 4 sources of the opposite polarity on the photosphere located in the loop's foot points [see *Titov et al.*, 2002, Figure 5–9]. The current sheet is located along the separator that is a field line connecting the two null points of magnetic field lines in the two interacting loops (flux tubes). The energy released inside a QSL has to be channeled to the photosphere by the surrounding field lines, so their convergent character at the end of QSL traces leads to concentration of the released energy and appearance of brightenings along the locations of reconnected magnetic lines [*Titov and Hornig*, 2002]. A magnetic inversion (neutral) line in the considered magnetic configuration with the two interacting sets of positive and negative polarities is associated with the location of a separator where the reconnection occur, that can be treated as an indicator of possible flare occurrence. The question remains how this quasi-steady magnetic configuration is disturbed in order to trigger a magnetic reconnection and energy release process.

[8] The magnetic inversion line (an apparent neutral line) was found to have a well distinguished sigmoid shape before a flare to occur, that is very often observed in the active regions producing solar flares [*Canfield et al.*, 1999; *Zarro et al.*, 2000]. This inversion line shape can be accounted for by more complicated reconnecting models with more than 4 magnetic sources like in the twisted flux rope model for two-ribbon flares [*Forbes and Isenberg*, 1991; *Amari et al.*, 2000] that can store a large amount of energy in a preexisting flux rope or by the tether-cutting phenomenological model [*Moore and LaBonte*, 1980] when the reconnection starts in a highly sheared core field and forms a flux rope as a result. The magnetic configuration with the preexisting eruptive rope is not stable for a long period and releases nearly all its energy into the interplanetary space during the eruption of this flux rope. The tether-cutting model can, possibly, allow to keep all the released energy to be kept inside the reconnecting magnetic loops without releasing it outside the Sun. Neither model predicts that any H_α or EUV emission appears prior to the eruption.

[9] On the other hand, the breakout model of magnetic reconnection [*Antiochos et al.*, 1999] predicts that a sheared core field pushes through an overlying restraining field starting a slow reconnection in the corona. After a substantial weakening of the restraining overlying field, the sheared core explosively erupts into the interplanetary space. At the same time, it stretches the remaining overlying field lines, which starts a fast reconnection beneath the escaping magnetic field releasing magnetic energy within a short timescale producing a flare and forming postflare loops in the eruption site. However, the breakout reconnection model is not expected to release much energy since the major part of it is stored in the underlying sheared field [*Antiochos et al.*, 1999]. This model also predicts appearance of EUV and remote H_α line brightenings in the foot points where the reconnecting field lines are embedded into the photosphere [*Sterling et al.*, 2001]. Hence the attempts to measure a reconnection rate from a slow speed of the H_α emission expansion in flare ribbons based on the breakout model

[*Isobe et al.*, 2002] produced some questionable results in terms of timing and total energy released in flares. The H_α ribbon expansion technique is most likely to measure the rate of energy deposition by fast energetic particles into dense chromospheric layers (or the ambient plasma heating) [*Somov et al.*, 1982; *Fisher et al.*, 1985] rather than the rate of magnetic field dissipation itself.

[10] *Yurchyshyn et al.* [2004] investigated the magnetic variations occurred in the 23 July 2002 flare long before and after the flare and their association with hard X-ray and H_α emission. On the basis of the movements of hard X-ray (HXR) sources for this flare, the emergence of a new magnetic flux is suggested that led to a magnetic reconnection and the HXR and gamma emission observed in this flare. The tether-cutting reconnection model [*Moore and LaBonte*, 1980] is proposed to explain the temporal variations of the magnetic field variations associated with the HXR and H_α emission from the wide area of the active region where the flare occurred [*Yurchyshyn et al.*, 2004]. The magnetic flux eruption was also confirmed by the TRACE observations [*Liu et al.*, 2003]. However, there were no energetic particles observed from this flare at the Earth orbit [*Gopalswamy et al.*, 2003], which points out onto a reconnection process occurring in the closed magnetic loops rather than in the open ones. Despite a good discussion of the multiwavelength emission in this flare provided by *Yurchyshyn et al.* [2004], who concluded the measured magnetic field variations to explain the observed locations and times of hard X-ray and gamma-ray emission, a detailed analysis of the magnetic field changes occurred during the flare itself still require more careful investigation. In the current paper we attempt to extend the research by *Yurchyshyn et al.* [2004] to a detection of the time lags between magnetic and hard X-ray changes and to establish the spatial locations of the HXR and gamma-ray sources where the magnetic energy was released during this flare.

[11] For this purpose the simultaneous observations of the flaring region by SOHO/MDI [*Scherrer et al.*, 1995], TRACE [*Handy et al.*, 1999] and RHESSI payload [*Lin et al.*, 2002] and by the BBSO high cadence H_α line images from BBSO are used. This flare has been actively investigated by the RHESSI team for hard X-ray and gamma ray sources [*Holman et al.*, 2003; *Krucker et al.*, 2002; *Lin et al.*, 2003; *Smith et al.*, 2003] and its energy balance deduced from the hard and soft X-rays [*Emslie*, 2003], which provides independent estimations to compare with.

[12] The data description is provided in section 2, the observed magnetic field variations are discussed in section 3 with the deduced reconnection rates and released energy presented in section 4.2. The conclusions are drawn in section 5.

2. Description of the Data

[13] This paper focuses on the correlation of magnetic field variations with the changes in hard X-ray emission in different bands from the loop top and foot point sources observed during the 23 July 2002 solar flare. The 2B/X4.8 flare occurred in the region located at S13E72 in AR NOAA 0039). It started in soft X-rays (GOES) at about 0015 UT and reached the peak flux at 0035:00 UT. The hard X-ray emission reached the first maximum at 0028:00 UT, the

second one at 0032:00 UT and the third one 2 min later (for the observed RHESSI light curves in this flare, see *Holman et al.* [2003, Figure 1] and the revised light curves in section 2.1).

2.1. RHESSI Images and Revised Light Curves

[14] For the present research hard H-ray images and light curves were built for the following RHESSI energy bands: $3-12$, $12-25$, $25-50$, $50-100$, $100-300$, $300-2000$ KeV. Several techniques were used for the RHESSI data reduction: the back-projection algorithm for the revised light curves and the CLEAN and PIXON procedures for the precise hard X-ray imaging required for overlapping with the MDI magnetograms.

[15] In order to connect hard X-ray (HXR) sources to the magnetic field changes the RHESSI light curves are rebuilt in each energy band measured from the identified sources, which occur within the area of the observed magnetic field changes (see section 2.3). For smooth light curves which are not affected by the insertion of shutters in the RHESSI instrument causing bumps in the light curves [*Smith et al.*, 2002] the series of 64 by 64 pixel RHESSI images were reconstructed in each band using the back projection algorithm for the whole period of the observations starting at 0020:00 until 0048.00. This algorithm provides a correct number of photons, despite giving a substantial distortion in imaging [*Lin et al.*, 2002], that is acceptable for the light curve restoration. For each energy band, series of RHESSI images were integrated over the same area providing a number of electron counts in the specified area.

[16] The parameters of the reconstructed images were as follows: the center of image in relation to Sun center x-coordinate: XCEN = −886.000, West and y-coordinate: YCEN = −237.000, North; width of pixel in data units CDELT1 = 1.00000 and height of pixel in data units CDELT2 = 1.00000. The X-ray images were resized and registered using bilinear interpolation to overlay correctly over the MDI images taken with different resolution. Then the hard X-ray pixel values were integrated over the rectangular area, which overlays the magnetic field changes. In the other words, revised light curves for the area marked with the mask of HXR sources were produced for every energy band.

[17] For the precise locations of the X-ray sources on the solar disk and their overlaying with H_α images and MDI magnetograms illustrated in Figure 1, more accurate imaging techniques were used: the PIXON procedure for the images taken in the energy band $12-25$ KeV and the CLEAN procedure for all other bands. Similarly to the RHESSI results [*Krucker et al.*, 2002], four sources were found, appearing at the maximum time 0028:45 UT (see Figure 1) which are referred to further as source A (far east from the ANL), source B (east-north from the ANL) and sources C (west-north from the ANL) and D (east-south from the ANL). The sources A, B and D were located on the negative magnetic polarity region and the source C on the positive polarity one (see section 2.3). Source A was the first to appear at 0028:00 UT in the $12-25$ KeV band and lasted until 0035:00 UT, decreasing in area with time. Sources C and D appeared at 0028 UT in the $12-25$ KeV band and then, another minute later, in the $25-50$ and $50-100$ KeV bands simultaneously with source B in the bands of $25-50$ KeV and higher.
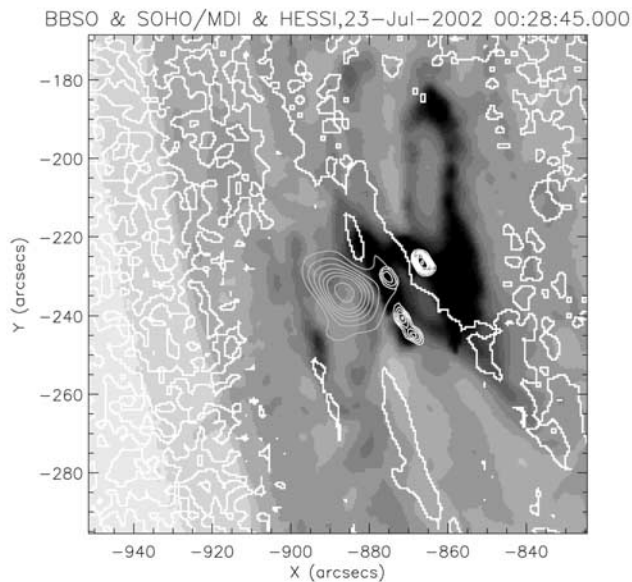
Figure 1. The RHESSI hard X-ray images (white thin contours) taken at 0028 UT overlaid on the MDI neutral line (NL) magnetograms (white thick contours) and H_α line images (negatives) taken at 0028:45 UT with the brightening loops (dark features around NL). The X-ray sources are referred as A (the most eastern), B (northeast), C (northwest), and D (southeast).

2.2. H_α High-Cadence Images

[18] The BBSO H_α images used are taken with 1 min cadence from 0022:00 UT until 0037:00 UT. In Figure 2 these images are overlaid with the magnetograms depicting magnetic inversion lines (ANLs) and the RHESSI images in the 25–50 KeV band and presented with one minute interval starting from 0026:45 UT (the top left image) to 0032:45 UT (the right bottom one).

[19] The H_α emission appears in the loops on both sides of an apparent neutral line (ANL) that can be called ribbons, one located on the west side (western loop, WL), which first brightens at 0022:00 UT in the southern end, and the other on the east side (eastern loop, EL) from an elongated ANL (see section 3.1), which appears much later at 0027:00 UT simultaneously with the start of hard X-ray emission. Later, at 0028:45 UT, these loops were connected by a third south-north loop (SNL) appearing growing in size across the elongated apparent neutral magnetic line from the location close to the southern leg of WL and the northern leg of EL embedded into the positive polarity island (see Figure 2, the first column). The brightening of the third loop (SNL), seen appearing from beneath of the first two, started at 0027:45 UT nearly coinciding with the first hard X-ray maximum in the 12–25 KeV band. This brightening keeps increasing in the eastern loop until the very end of the H_α observations while in the western loop it became much fainter toward the end (Figure 2, the last two columns).

[20] The location of the hard X-ray source C is in the middle (possibly, top) of the eastern loop in the H_α images and the hard X-ray source B is located in the middle of the SNL loop (see section 2.1). The southern foot point of the eastern loop seems to be close to the location of the X-ray source D. Source A does not have any links with the H_α emission.

[21] The H_α spectral observations of this flare also revealed the mustaches with a strong line inversion [*Firstova et al.*, 2003] observed at 0032:00 UT, just after the second maximum in hard X-rays, in the location of hard X-ray foot point B according to their slit position. The linear polarization of 3–10% with the plane of polarization parallel to the solar center direction is attributed to impact polarization that clearly indicates the presence of fast electrons propagating into the X-ray B foot point located in the eastern ribbon where the slit was placed.

2.3. SOHO/MDI Magnetograms and White Light Images

[22] The magnetograms were obtained with the Michelson Doppler Imager aboard SOHO in the full disk mode (1024 by 1024 pixels) taken every minute starting at 0010:00 UT until 0059:00 UT and synchronized to the Earth viewpoint [*Scherrer et al.*, 1995]. The MDI data, obtained from the nine filtergrams taken in pairs to minimize the effect of possible intensity variations (for details, see also *Scherrer et al.* [1995]), were used to calculate the line shifts in both polarizations using a Fourier tachometer method for the estimations of a LOS magnetic field magnitude. Owing to the flare location S13E72 near the eastern limb, the LOS magnetic field component measured by MDI was closer to the horizontal than the vertical. The MDI white light images are constructed at 4 per day, and the nearest one was taken at 2359:00 UT on 22 July 2002. This MDI image was used for sunspots detection and their coalignment with the magnetic field magnitudes, the locations of the ANL and RHESSI hard X-ray sources (see Figure 3).

[23] The northern leg of the large western loop (WL) (see Figure 2, the first column) begins from the location of a sunspot with the positive magnetic field of 620 G and the southern leg of WL is connected to another sunspot with the negative field of −570 G, which is located close to the magnetic island of 100–200 G of the positive polarity. The western loop looks rather high because of its well-defined loop structure and the large distance from its top to the foot points. The northern leg of the eastern loop (EL) is connected to a positive polarity island above located on the north in the negative-dominated region and the southern leg is embedded at the location of the strong (−370 G) negative magnetic field.

3. Observed Magnetic Field Variations

[24] The apparent neutral magnetic line (ANL), which separates the opposite magnetic polarities of the LOS magnetic field component (nearly horizontal for this flare location, see the remarks in section 2.3), was also identified for all 50 MDI magnetograms taken during this hour. The floating point data of the LOS magnetic field in the magnetograms in a small area 120 × 120 pixels around the flare location was magnified in size by factor four using bilinear interpolation. The magnified images are converted to a binary form by applying a threshold of 0.0 G, the boundary between the positive and negative polarity regions
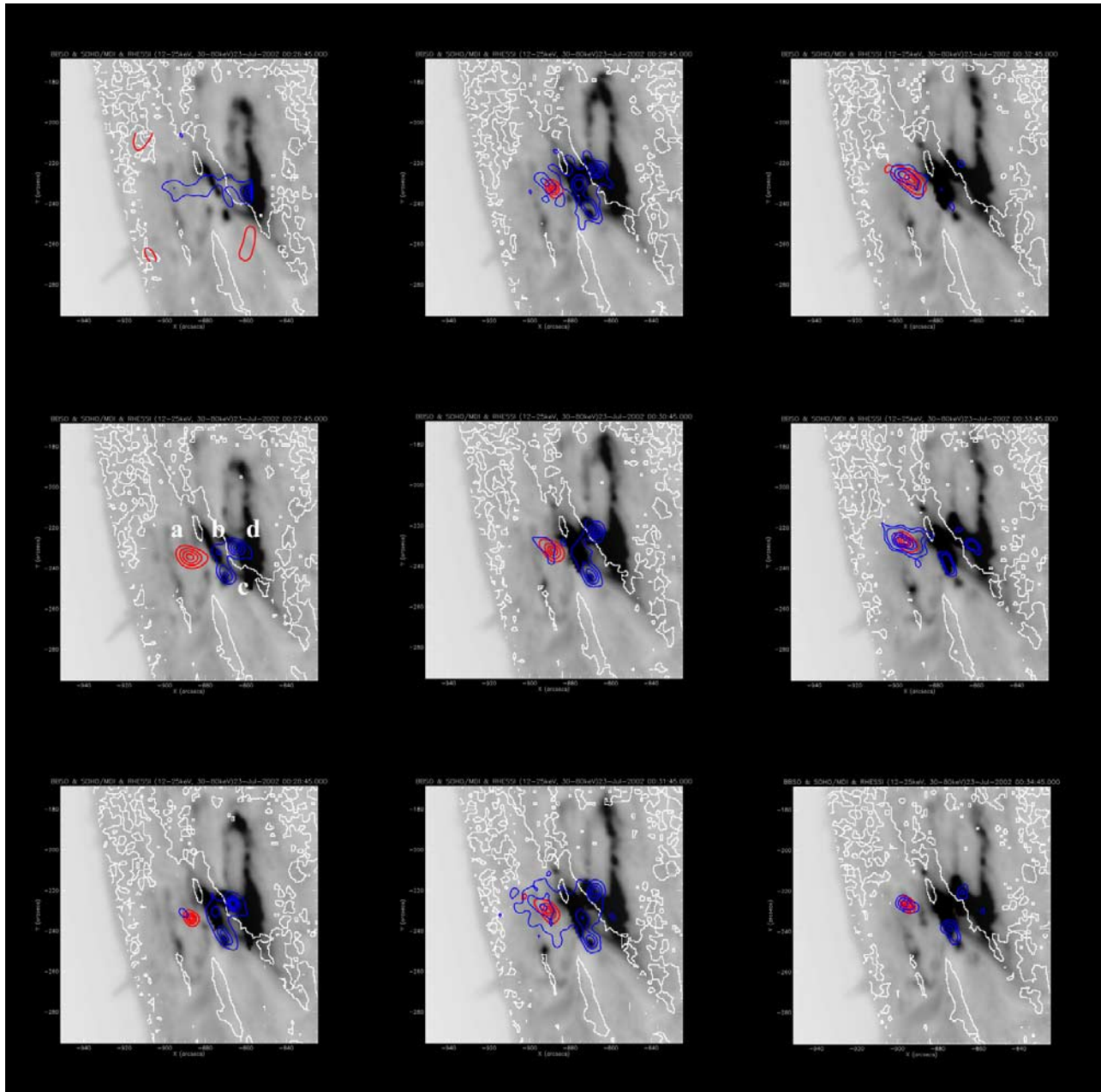
Figure 2. The RHESSI hard X-ray images (red contours, 12–25 KeV band; blue contours, 50–100 KeV band) overlaid on the ANL map obtained from the MDI magnetograms (white lines) and H_α line loops (dark black) taken with 1-min cadence from 0026:45 UT (the upper left image) until 0034:45 UT (the right bottom image).

corresponding to the ANL was marked using a morphological edge detector.

3.1. Discharge of Magnetic Field

[25] From the quick-look RHESSI images an approximate location of the flare was established and the MDI images were cropped to cover an area around the flare location. The cropped images (50 in total) were put into a movie with the mpeg movie software, which revealed the existence of flare-related magnetic field variations via a negative polarity discharge across the flaring area appearing at 0025:00 UT, or 3 min before the first hard X-ray maximum, and finishing after 0038:00 UT.

[26] This is an indication of fast magnetic field changes occurring during the flare, which we further investigate from the difference magnetograms presented in Figure 4. The cropped images of the differences between the MDI full disk magnetograms taken every minute with its number shown in the left corner, and the full disk magnetogram at 0020:00 UT before any signs of the flare onset. The grid shows the same pixel locations for every difference magnetogram cropped from the full disk ones.

[27] The black blob above the 4th horizontal and to the right from the 2nd vertical grids shows a big negative magnetic discharge seen every minute moving away from the flare site in the magnetogram movie. The magnetic
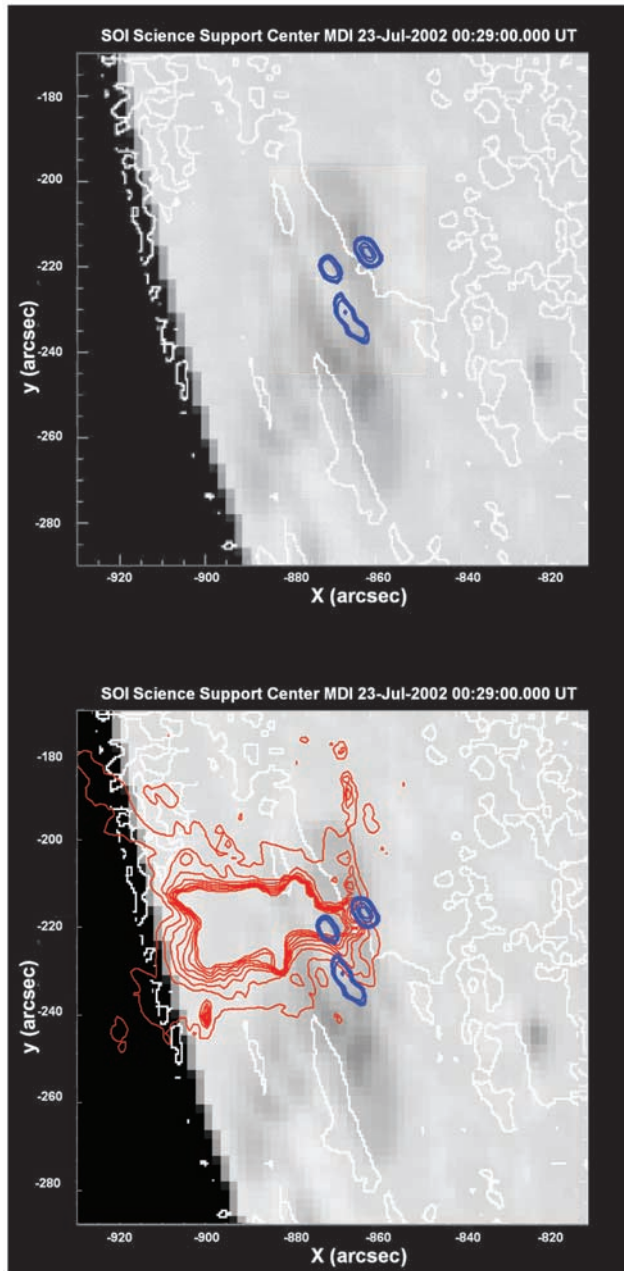
Figure 3. (top) The RHESSI hard X-ray images obtained in the band of 40–80 KeV (blue contours) at 0029 UT overlaid on the MDI magnetograms with the ANL (white lines) and the MDI white light image with sunspots (dark areas around the ANL) taken at 2359:00 UT on 22 July 2002. (bottom) Same as above, with the TRACE loop contours (red) taken at the same time.

movement is not noticeable in the 24th and 25th segments while in the 26th one can see a first appearance of the negative blob located just above the 4th horizontal grid. From the segment 26 onward the blob is constantly growing in size above the original location and keeps growing to the segment 32 and beyond until the end of the flare at 0045:00 UT (not shown here). This appearance of a new emerging flux in this flare favors the tether-cutting model suggested by *Yurchyshyn et al.* [2004].

3.2. Total Magnetic Field Variations

[28] In order to measure quantatively the magnetic field variations near the flare location, a rectangular box was determined encompassing the area along the apparent neutral magnetic line and used as a mask for integration (summing up) of the values of magnetic field in every image. The mask included the locations of the two major sunspots of positive (500 G) and negative (−650 G) polarities, a few locations of increased magnetic field above 200 G located along the apparent neutral line and the background magnetic field ($\prec$20 G). Magnetic field variations in this area are presented in Figures 5 and 6 (upper graphs).

[29] For quantitative estimation of any possible connection between these variations and the increase of hard X-ray emission a cross-correlation analysis with a time lag was carried out between the magnetic variations measured in the central rectangular mask and the updated hard X-ray light curves (see section 2.1), obtained in all the bands for the times between 0020:00 and 0035:00 UT. The magnetic changes, HXR light curves for 12−25 KeV and 0.3−200 MeV, respectively, and their cross-correlation
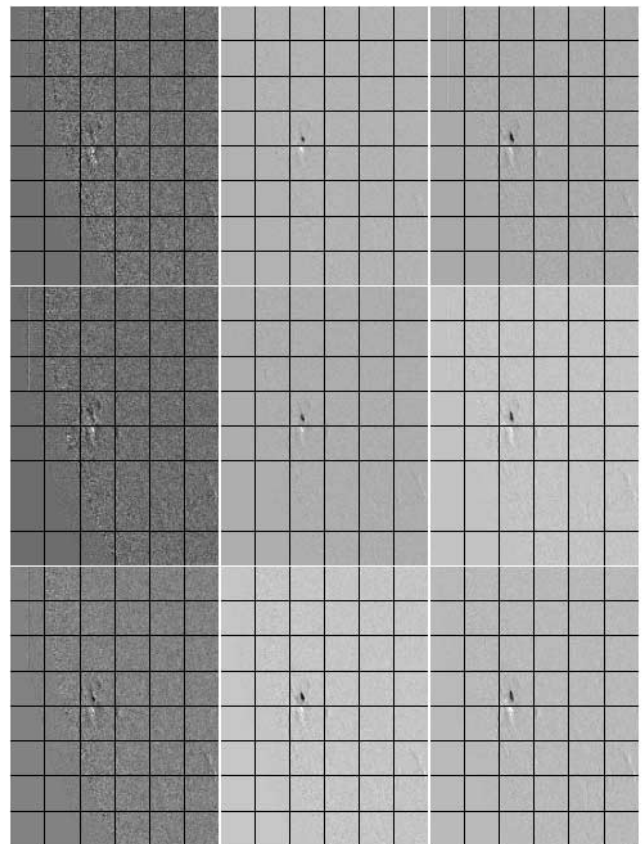

Figure 4. The MDI cropped difference magnetograms taken with the magnetogram at 0020:00 UT subtracted from the original full disk magnetograms taken every minute (by columns from the left top corner) from 0024:00 to 0032:00 UT. The grid shows the same pixel locations for every difference magnetogram cropped from the full disk ones. The black blob above the fourth horizontal grid shows a big negative magnetic discharge seen in the magnetogram movie.
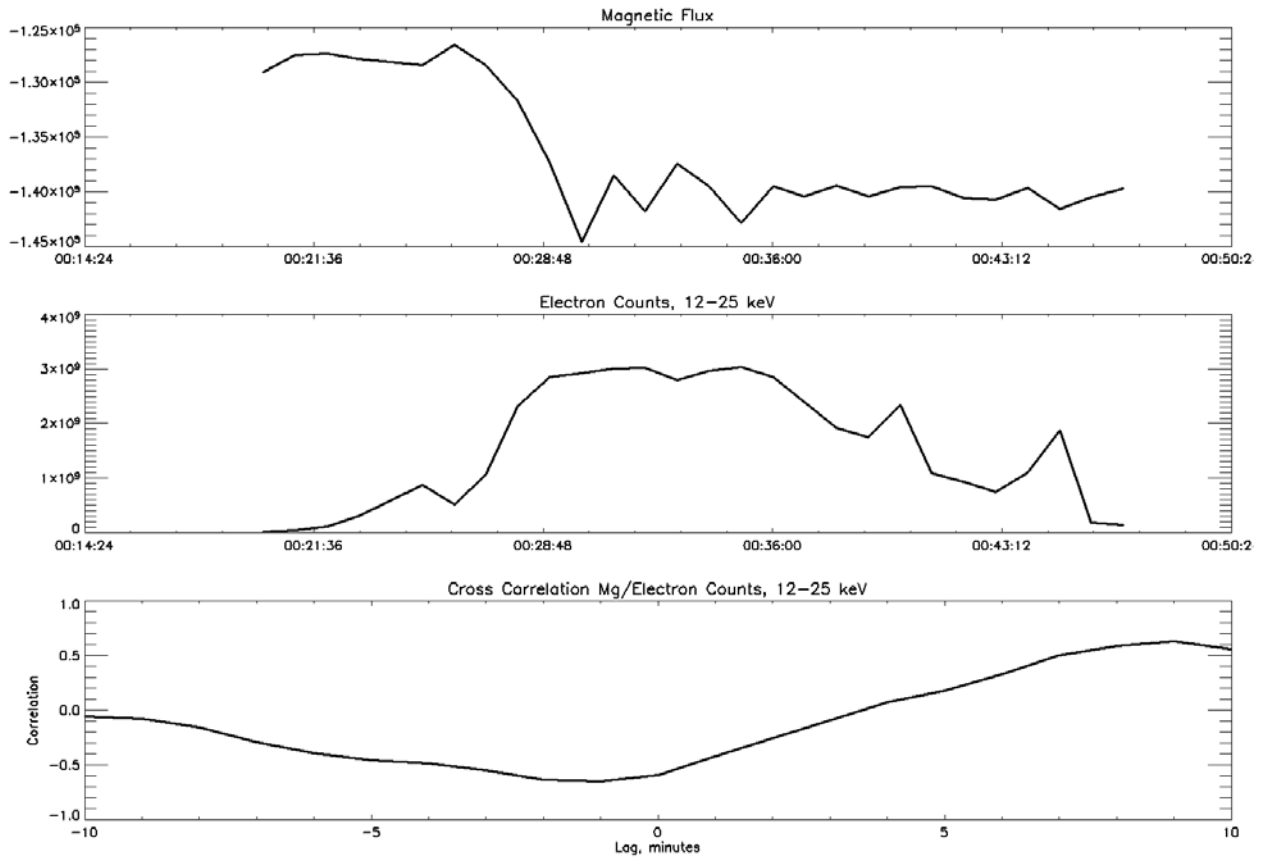
Figure 5. (bottom) The time lag cross-correlation coefficients between (top) the total magnetic flux variations in the rectangular area around the flare prior and (middle) during the flare and the RHESSI hard X-ray light curve in 12–25 KeV band.

coefficients for different time lags are plotted in Figures 5 and 6 versus the lag times starting from 0020:00 UT during the whole flare duration. The hard X-ray emission in the 12–25 KeV band starts at 0025:00 UT, or 2 min later than the magnetic field changes, and reaches its first maximum at 0028:00 UT that is also shown in the paper by *Yurchyshyn et al.* [2004]. However, the cross-correlation coefficient between the magnetic and hard X-ray variations in this band for different time lags increased from 0 at the time lag 0 (or 0020:00 UT) to 0.5 at the time lag of 9 min (0029:00 UT) that coincides with the first maximum of the hard X-ray emission in 12–25 keV band. The emission in the higher energy X-ray band (0.3–200 MeV) starts at 0026:00 UT that is 1 min later than those in 12–25 keV band. However, its time lag cross-correlation coefficient with the magnetic field changes increases from 0 at the time lag of 1 (0020:00 UT) to 0.6 at the time lag of 7 min (0027:00 UT) that coincides with the start of the magnetic discharge discussed in section 3.1. What is interesting that the nonzero cross-correlation coefficient is shown for the higher energy band starting from the time lag −1 min, or at 0019:00 UT and stays at nearly the same level for another 9 min, i.e., until 0028:00 UT after which it sharply drops down again. This, possibly, reflects the acceleration of particles inside the primary reconnecting region to very high energies [*Zharkova and Gordovskyy*, 2004] during a reconnection stage in the upper magnetic loops which was disrupted, possibly, by a magnetic field eruption. The cross-

correlation coefficient for a lower energy band steadily increases from 0.1 for a lag time of 0 to the maximum 0.5 at the lag of 9 min (0028:00 UT) and begins slightly decreasing after this time. This can indicate a steady generation of electrons within this energy band during the magnetic field line reconnection in lower magnetic loops, that is not affected by the magnetic field eruption.

[30] For more precise detection of these magnetic variations a narrower mask associated with the locations of hard X-ray sources was selected (see Figure 7 (top plot, central mask)). Although this mask was much smaller than in the previous rectangular area around the flare (Figures 5 and 6), the magnetic field changes within this mask showed the same behavior as for the wider one. The total magnetic flux from the wider area was not much different from those measured for the narrower central mask as per Figure 7 (top). In order to check, if the magnetic field variations are associated with the specific magnetic topology in the vicinity of the ANL, the mask was moved beyond the neutral line to the positive or negative polarity regions (see Figure 7 (top), the left and right masks), and the magnetic flux integration was repeated. The temporal variations of the integrated LOS magnetic flux in the areas of each mask are plotted in Figure 7 (bottom).

[31] The measured total LOS magnetic flux from the rectangular mask (Figures 5 and 6) as well as from a smaller area covered by the central mask area (Figure 7) is negative;
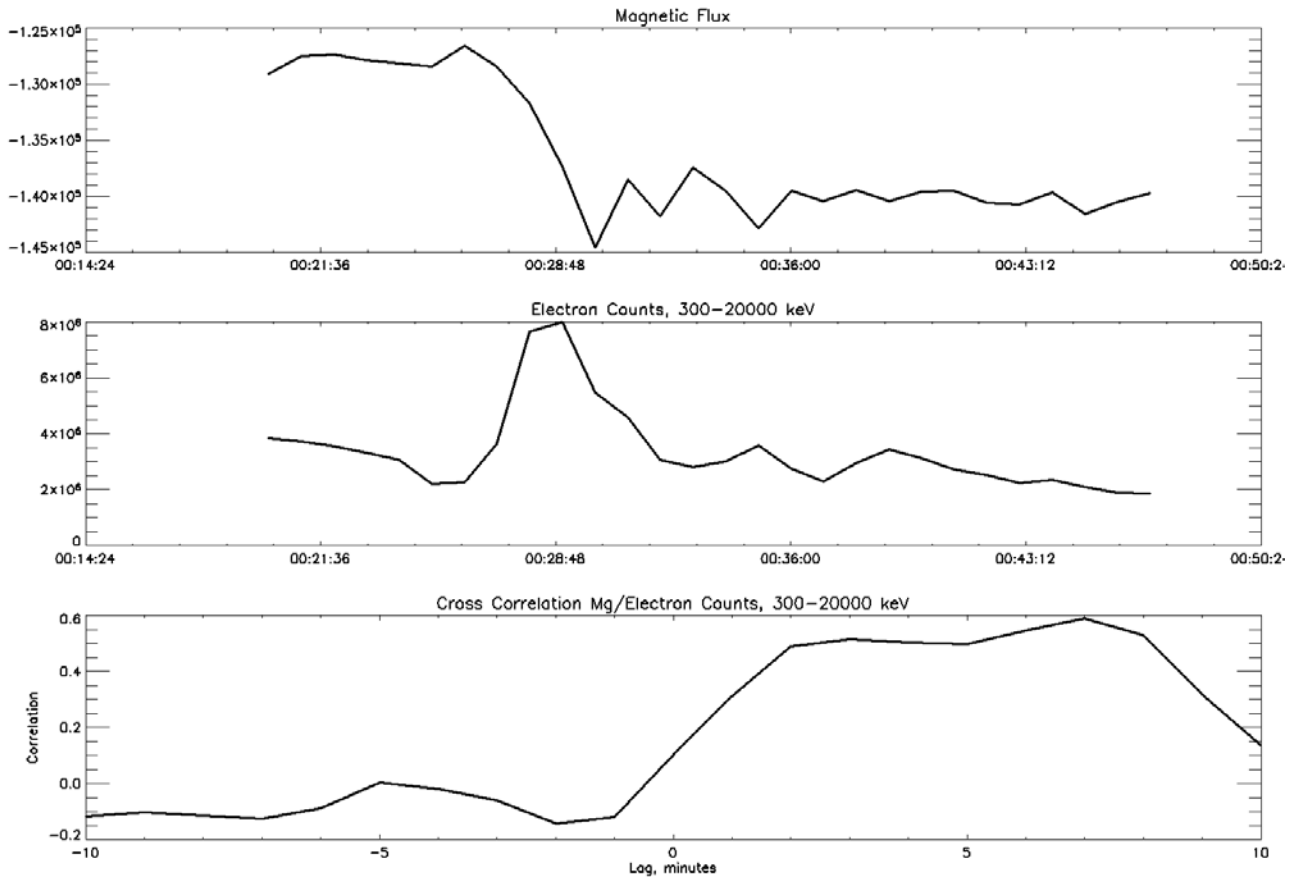
Figure 6. (top) Cross-correlational coefficient between the total magnetic flux variations in the same area as in Figure 6 (middle) prior and during the flare and (bottom) the RHESSI hard X-ray emission measured in the band 0.300–2 MeV.

it slightly decreased before the hard X-ray flare onset at 0023:00 UT and then steadily increased until 0030:00 UT. As can be seen, only in the area of a central mask, that includes the apparent neutral magnetic line, the magnetic flux was found increased by the factor 4 (or by ~120 G in magnetic field strength), that significantly (by factor 6) exceeds the background magnetic field of 10–20 G. The magnetic field changes are irreversible, the magnetic field reaches a new level of the steady state and does not return to a preflare value that is similar to the magnetic field changes found for the regions 1 and 2 in the Bastille flare 2000 [*Kosovichev and Zharkova*, 2001]. The magnetic flux in the two areas covered by the other masks (in either positive or negative polarities) does not show noticeable variations above the noise level.

[32] However, there are no clear indications from the LOS magnetic field measurements presented above that a secondary reconnection occurred later as suggested by *Yurchyshyn et al.* [2004]. The major total magnetic field variations appear prior and during the first HXR maximum at 0028:00 UT with rather small fluctuations around the time of the secondary HXR increase. There are, possibly, some additional magnetic changes not measured by the LOS magnetic field but only by the full vector measurements as reported by *Yurchyshyn et al.* [2004] when the longitudinal component becomes a transverse one. Hence we cannot confirm or deny the secondary reconnection from the LOS

measurement of magnetic field changes in the whole area. Yurchyshyn et al. also pointed out that the direction of the positive magnetic field arrows are changed from the west-east (before flare) to the one from the southwest to the northeast (after the flare), which was interpreted as more evidence of the exchange between the longitudinal and transverse magnetic field components. However, these changes are also close to the directions of the reconnected magnetic lines expected from the global reconnection models discussed in section 4.1 and Figure 11. In order to clarify this point, let us investigate the LOS changes locally, i.e., on the magnetograms of the flaring area inside the HXR sources and the magnetic sources in the whole area.

3.3. Local Magnetic Field Variations

[33] In order to identify the narrower areas of the sources of a magnetic energy release, we try to use the established correlation of magnetic changes with hard X-ray emission. In particular, the precise RHESSI hard X-ray images in the 40–80 KeV band (see section 2.1) with four hard X-ray sources appearing during the course of the flare similar to the locations in the paper by *Krucker et al.* [2002] were overlaid onto the MDI magnetograms. The magnetic flux variations were extracted from the maximum areas covered by this hard X-ray emission for each minute before and after the flare onset for each hard X-ray source A-D and are presented in Figure 8.
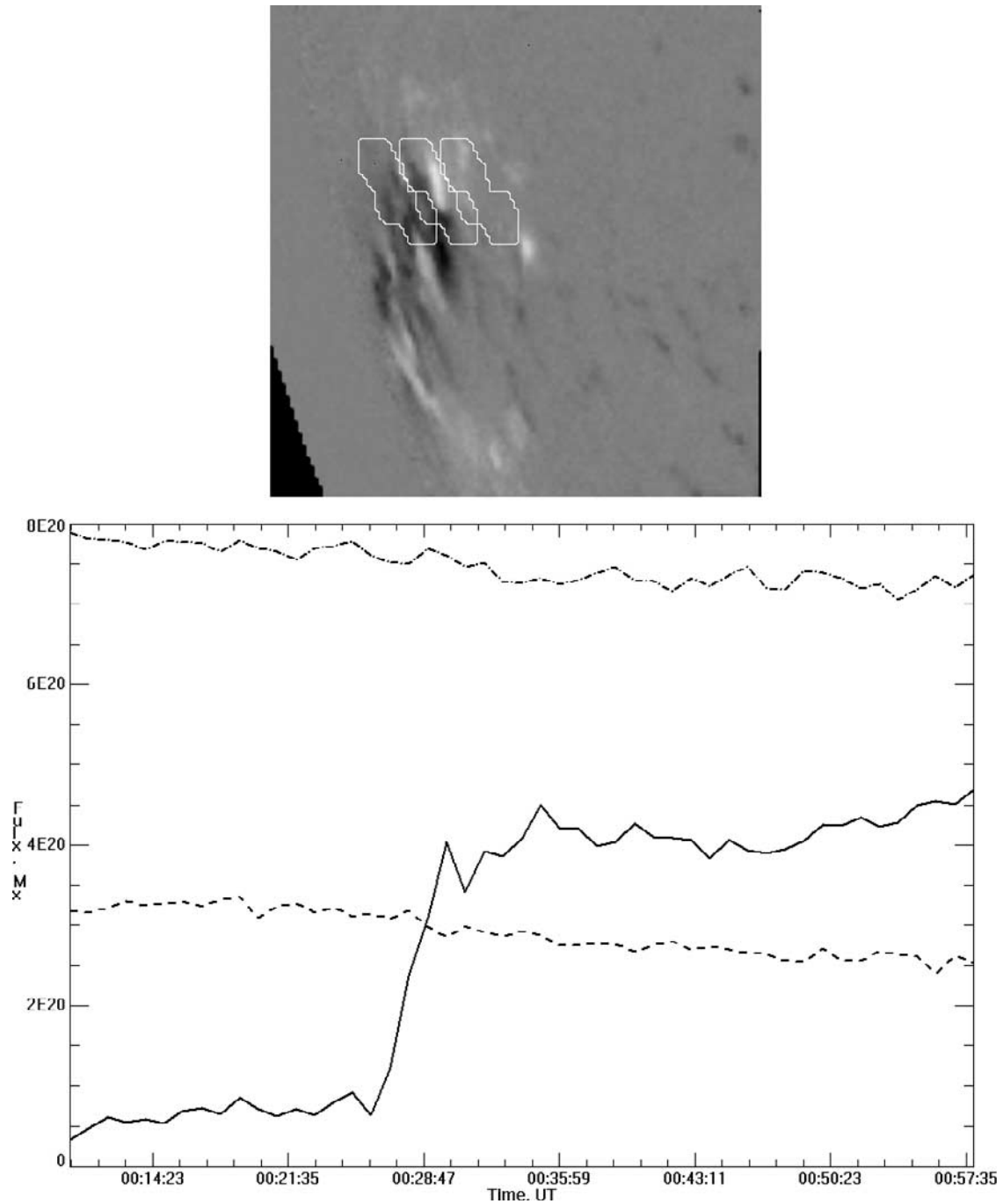
Figure 7. The total magnetic flux variations (in Mx) from the flare of 23 July 2002. (top) The mask locations on the magnetograms: mask 1 (left) only the negative polarity; mask 2 (middle) including the magnetic inversion (neutral line); and mask 3 (right) only the positive magnetic polarity. (bottom) Corresponding total magnetic flux variations (dashed line, left mask; solid line, middle mask; dashed-dotted line, right mask).

[34] The source A is found not to be associated with any magnetic field changes, despite appearing in the 12–25 KeV band 1 min earlier than the other foot point sources B, C and D, but still 1 min after the start of the magnetic changes. In the source D (bottom source) and B (middle source), situated on the negative magnetic polarity sides from ANL, the magnetic flux increase is permanent, or irreversible. The magnetic field in the sources B and D starts increasing at 0026:00 UT and continue for 3 min until it stops 1 min later after the maximum of the first hard X-ray burst at 0028:00 UT at the magnetic field magnitude reached during this increase. After 0029:00 the magnetic field retains this level. The temporal variations of magnetic field in the sources B, C and D are presented in Figure 9 (from the top to the bottom, respectively).

[35] The source A is most likely a projection of the top of the loop (see the TRACE image overlaid onto the H_α image,
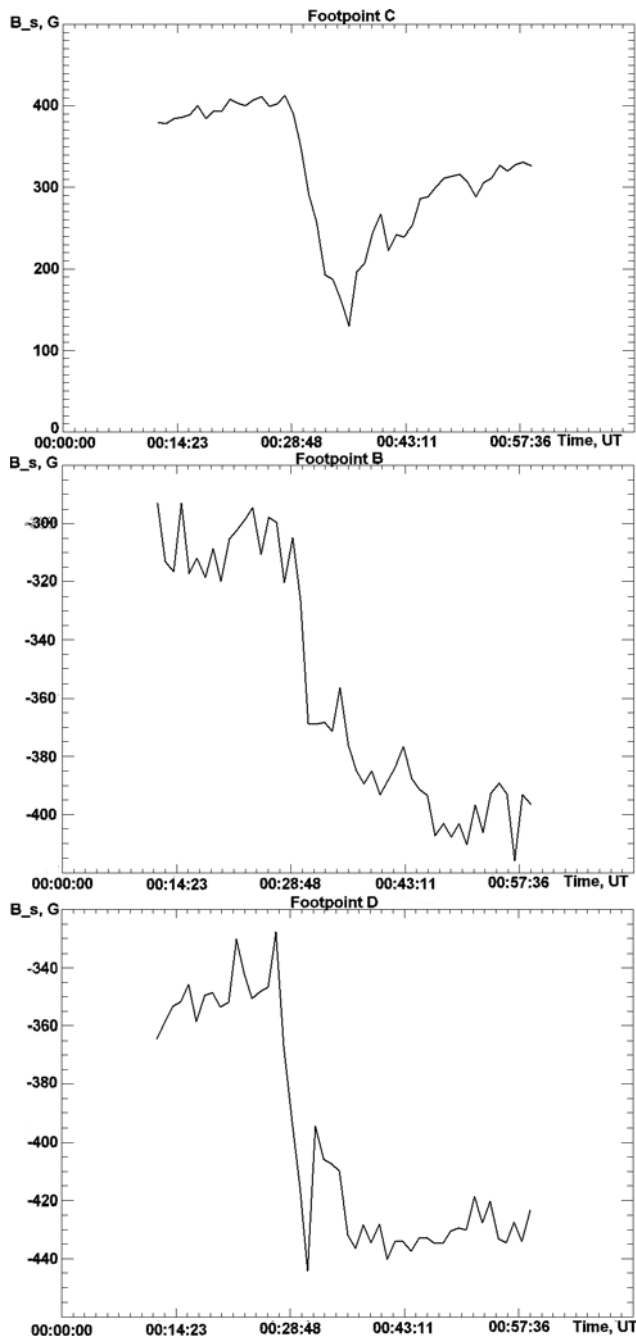
Figure 8. The summated magnetic field variations (B_s in G) in the locations of hard X-ray sources (bottom) D, (middle) B and (top) C. The sources A, B, C, and D are defined in Figure 1 and section 2.1.

(Figure 3, bottom); the loop is embedded into the photosphere at the locations close to the foot points (sources B, C and D, see section 2.1). The source A can be a good candidate for the site of primary electron acceleration in this flare because of the hard X-ray emission timing, its energy and relation with the radio emission discussed by *Krucker et al.* [2002]. However, it does not show direct connections with the magnetic field locations, possibly, because of its occurrence on the loop's top and the loop tilt toward the limb. On the contrary, the sources B, C and D

are clearly the foot point locations and, hence, their connection with the magnetic field changes are much more pronounced. The changes in foot points B and D are fully irreversible, the magnetic field in them decreasing from -300 to -420 G; the source D has these changes from 0026:00 UT for 2 min which then at 0029:00 UT are followed by the magnetic changes in the sources B and C lasting for 2 and 4 min, respectively.

[36] In the source C the magnetic changes are mostly reversible with the magnetic field first decreases from 400 G to 100 G and returns to about 300 G after the flare (Figure 9, bottom). Since in the source C a difference between the new level of magnetic field, achieved after any changes were stopped, and the preflare level is close to the magnitude of irreversible changes measured in the foot points B and D, we can conclude that these changes are partially irreversible. The major part of these magnetic variations in the source C are reversible of the transient type, similar to those found by *Patterson and Zirin* [1981] and are not real magnetic field changes but caused by a short-term increase of the line intensity, possibly, caused by a nonthermal excitation by high-energy electrons of the upper level of the Ni atom in the transition 6768 Å (for details, see *Zharkova and Kobylinsky* [1993] and *Zharkova and Kosovichev* [2002]).

[37] There are also other indications for the presence of high-energy electrons at the location of the source C, in the H_α spectral observations of this flare, which revealed the mustaches appearing at 0032 UT just after the maximum in hard X-ray emission in the location of the foot point C according to a slit position [*Firstova et al.*, 2003, Figure 1]. The H_α line at these locations had a strong line inversion, its linear polarization was about $3-10\%$ with the plane of polarization parallel to the solar center direction. This confirms the presence of fast electrons which propagate in the plane of the solar image resulting in the plane of polarization being perpendicular to the observer [*Zharkova and Syniavskii*, 2000; *Karlicky and Henoux*, 2002].

[38] Therefore from the LOS magnetic field measurements presented above it is clear that the secondary reconnection did not occur inside the 3 HXR sources associated with the foot points, which confirms the conclusions by *Yurchyshyn et al.* [2004]. These authors also pointed out that the direction of the positive magnetic field arrows is changed from west-east (before the flare) to the one from southwest to northeast (after the flare), which was interpreted as more evidence of exchange between the longitudinal and transverse magnetic field component. This exchange can be a part of the magnetic reconnection process that leads to the reconnection of magnetic field lines from one loop to another as suggested by the global reconnection models discussed in section 4.1 and Figure 11. Thus let us have a look at the changes in the magnetic sources present in the whole area around the flare.

3.4. Magnetic Sources and Discharge Movements

[39] The negative blob, or magnetic discharge, discussed above in section 3.1 did not exist prior the flare onset but appeared during the course of the flare 7 min after the magnetic changes started. It moves in the northeastern direction, and during its expulsion it crosses the apparent neutral magnetic line (ANL) in the magnetic configuration
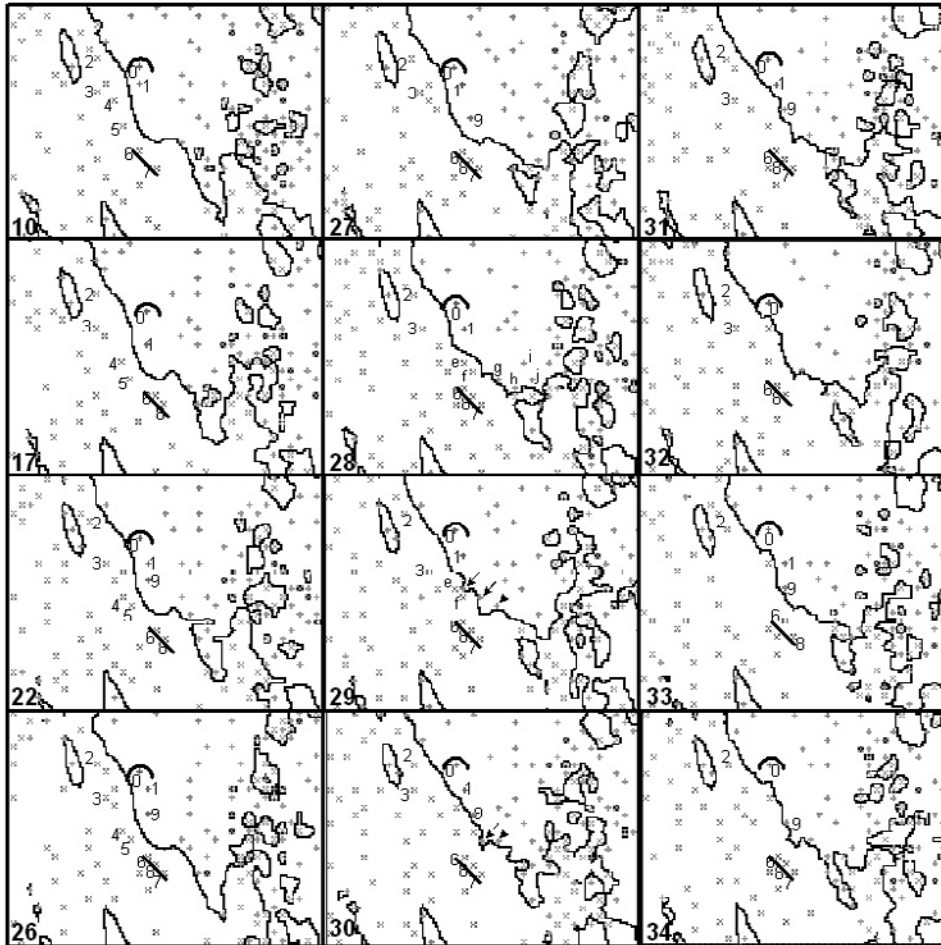
Figure 9. An evolution of the locations of strong magnetic sources with respect to the neutral line movement prior and during the X-ray emission (pluses define positive sources; x define negative ones). The magnetic field of the sources in G at 0028:00 UT is 0, +620; 1, +550; 2, −270; 3, −340; 4, −370; 5, −350; 6, −570; 7, −560; 8, −600; 9, +300. The newly emerged magnetic sources are: e, −580; f, −380; g, +110; h, +50; j, +130; i, 160. The sources 0−3 and 6−8 stay nearly in the same locations; the sources and 4−5, 9, and 8 move (see the text); and the sources e−i just appeared.

around the flare and keeps moving to the north for another 13 min. This confirms that the magnetic reconstruction process in this particular flare was close to the phenomenological tether-cutting model as concluded by *Yurchyshyn et al.* [2004].

[40] In order to understand the magnetic topology on the photosphere, we have extracted the locations of magnetic source with maximum fields with magnitudes exceeding by ≥100 G the average magnetic field of neighboring 9 pixels. These sources are presented in Figure 9 for the following UT times (minutes after midnight): 10, 17, 22, 26−34 that captured the major preflare magnetic field changes and those that occurred during the flare itself. As can be seen, there are 10 preexisting sources (0−9) and 6 newly emerged ones (e−j). The magnetic field magnitudes of the sources (in G) at 0028:00 UT are 0: +620, 1: +550, 2: −270, 3: −340, 4: −370, 5: −350, 6: −570, 7: −560, 8: −600, 9: +300. The newly appeared magnetic sources have the following magnetic fields (G): e: −580, f: −380, g: +110, h: +100, j: +130, i: 160.

[41] The preexisting sources are divided into the two classes: the stable and moving ones. The stable sources,

which are merely stationary (±2 pixels), are: on the north of ANL: 0 for positive polarity and 2−3 for the negative polarity; on the south of ANL: 6−7 for negative polarity. The moving sources are 1, 4, 5, 8 and 9 which start moving prior to and keep moving during the flare occurrence. There are also 6 new sources e−j which appeared just 2 min prior to the flare at 0026:00 UT at very close locations to the ANL, 2 at the negative side and 4 at the positive side. The new emerged sources of negative polarity have much higher magnetic field than the positive ones.

[42] Prior to the flare, from 10 to 22 min past midnight, in the northern side of the ANL the negative polarity sources 4 and 5, which later became close to the RHESSI source B, started moving by 4−6 pixels to the south. At the same time, the positive source 2 slightly moved to the south as well and the source 9 suddenly appeared at 0022:00 UT (Figure 9, the first column) in the location which later was established for the RHESSI source C. Over a similar period from 10 to 26 min in the southern side of ANL the two sources with magnetic field of −570 G and −510 G appeared below the sources 6−8, which later coincided
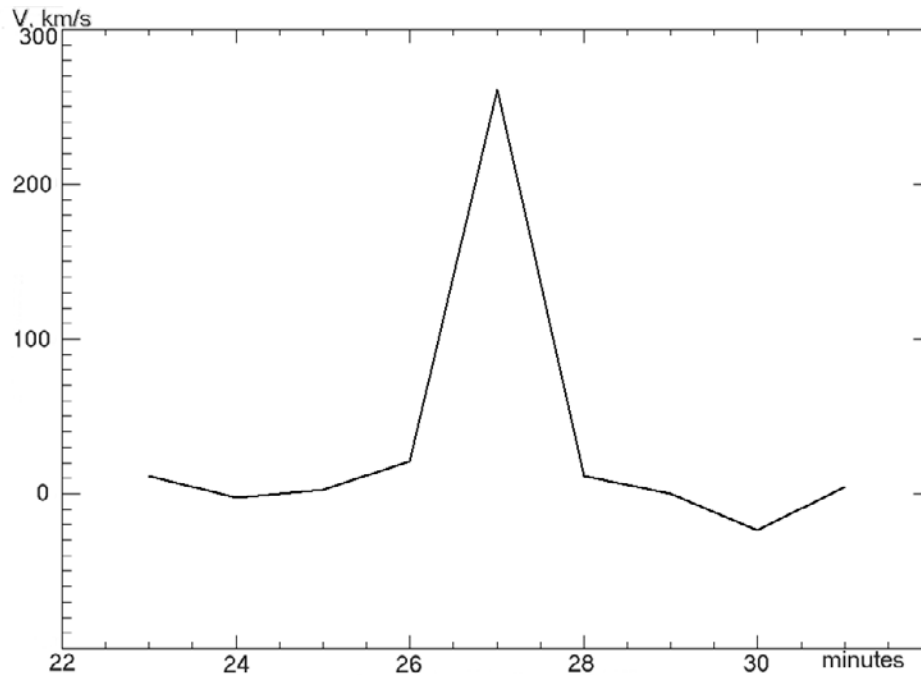
Figure 10. The speed variations of a neutral line movement as a flat image projection of the magnetic field discharge discussed in section 3.1.

with the RHESSI source D, but not with the existing negative sources 6–8 associated with the negative sunspot as seen in H_α images (see section 2.2). These sources started moving toward the sources 6–8, and at 0026:00 UT all the negative sources were located just in front of the ANL bump toward the negative polarity (Figure 9, the second column).

[43] At 0027:00 UT (Figure 9, the second column) the ANL is pushed to the positive side by 12 pixels in comparison with its location at 0026:00 UT but there are no sources clearly seen near this ANL location, while the source motion is registered on the southern part of ANL with a new island of positive polarity formed just below the locations where the 4 new positive sources appeared a minute later. At 0028:00 UT the new negative polarity sources e and f emerged very close to the ANL and the new positive sources g, h, i and j appeared on the far south side of the ANL. These new emerged sources pushed the ANL to a nearly straight line shape at the same time when the total magnetic flux starts increasing (see Figures 5 and 6 (upper plots), Figure 7 (bottom), and section 3.3).

[44] The initial magnetic field changes start in the southern foot point of the western loop (Figure 2, the first column), which was followed by the appearance of a new loop (SNL) across the ANL reported in section 2.2, which was seen rising in height. The new source locations coincide in space and time with the appearance of this SNL. The newly emerged sources existed for another 2 min until the hard X-ray maximum and then at 0031:00 UT disappeared at this location but moved further north. Another fast change in the ANL shape occurred at 0032:00 which was again followed by a secondary (but smaller) increase of hard X-rays, which had a smaller scale and, hence, was more difficult to

follow in Figure 9 (the last column). Particularly, in the sources B and D there are irreversible magnetic field changes indicating a pure magnetic field dissipation while in the source C the changes are partially reversible pointing to a presence of high-energy electrons.

[45] Hence, by evaluating the displacement of the apparent neutral line (ANL) caused by the projection effect of the magnetic flux expulsion onto a flat solar image, one can measure the speed of the negative discharge presented in Figure 4. This discharge reflects a magnetic reconnection in the global reconnection models applicable for this flare (see section 3.2 and *Somov* [2000] and *Titov et al.* [2002]) and the speed variations of this expulsion measured from the ANL movement are presented in km/s in Figure 10. The ANL starts moving at 0026:00 UT that is 2 min before the flare first X-ray maximum, then at 0027:00 its estimated speed approaches a maximum magnitude of 250 km/s. This is about 5–10% of the local Alfven speed in the corona for density of 10^{10} cm^{-3}, that fits very well into the theoretical predictions of a reconnection speed V_i by *Priest* [1984] and *Somov* [2000].

[46] These changes in the magnetic source and ANL locations clearly point out to the processes of magnetic reconstruction with the expulsion of magnetic field that was previously noted by *Yurchyshyn et al.* [2004] from the movement of the HXR sources. This emerging flux confirms the conclusions about the tether-cutting model applicable for this flare reconnection scenario b [*Yurchyshyn et al.*, 2004]. This expulsion can initiate a smaller-scale reconnection in the higher magnetic loops in or above the HXR source A (not observed by MDI measurements), which is not associated with a magnetic source on the photosphere within the considered area but still led to
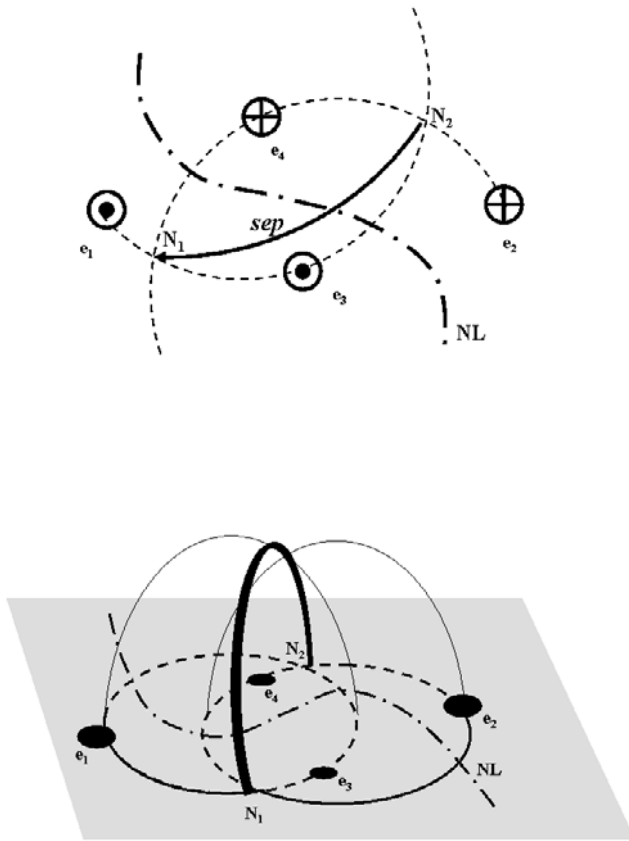
Figure 11. (top) The photospheric positions of LOS magnetic model sources $e_1 = -e_2 = 0.6$ and $e_3 = -e_4 = 0.4$ [from *Titov and Hornig*, 2002]. (bottom) The position of a separator field line (solid line) formed by 4 point-like sources connecting the two null points formed by the intersection of separatrix surfaces (thin dome-like lines connecting the photospheric sources) [from *Sweet*, 1969; *Titov and Hornig*, 2002].

another HXR maximum reported for this flare [*Lin et al.*, 2003].

4. Estimations of the Energy and Magnetic Reconnection Rates

4.1. Theoretical Background

[47] In order to understand what one can measure from the LOS magnetic observations, let us use a description of the magnetic line connectivity in the quasi-separatrix layers (QSLs) [*Titov et al.*, 1999, 2002] based on the global reconnection models formed by two interacting magnetic loops embedded into the photosphere at the 4 foot points (sources), two each of the opposite polarity [*Sweet*, 1969; *Gorbachev and Somov*, 1988] (see also *Titov et al.* [2002, Figure 11]).

[48] In Figure 11 a quasi-static model of magnetic structure that exists prior a reconnection start and at each moment during it is plotted. In the top plot there is a schematic presentation of four photospheric sources: the two existing stronger sources $e_1 = -e_2 = 0.6$ and two newly emerging weaker sources $e_3 = -e_4 = 0.4$ (Figure 11, top), each pair of which are connected each to other prior a flare in such a way that their magnetic structures intersect at the

QSL surfaces presented in the Figure 11 (bottom) by the dome intersections at the null points N_1 and N_2 on the photosphere. The intersection of these QSL surfaces is a separator that is a field line connecting the two null points N_1 and N_2 of the QSL magnetic field line intersections located on the photosphere. The separator, or a quasi-separator defined by *Titov et al.* [2002], is the location where a current sheet is formed and a reconnection can occur. The region of the maximum in each polarity corresponds to the photospheric cross sections of this QSL, called a QSL trace. This is a narrow strip of the separator passing above the inversion line (magnetic neutral line) in the idealized model in Figure 11.

[49] The violation of a quasi-static condition in the simple 4 source model presented in Figure 11 (top), can be caused either by motion of one of the sources or by magnetic field twisting in the other one. This, in turn, can initiate a reconnection of magnetic field lines in a diffusive region of the current sheet appearing above the separator [see *Priest*, 1984] (Figure 12). In a very simple approach, the variations of the magnetic flux $B_i \times V_i$ entering the current sheet in this diffusive region can be measured by the changes of the outcoming magnetic flux $B_o \times V_o$ as follows [*Priest*, 1984]:

$$B_i \times V_i = B_o \times V_o \qquad (1)$$

where V_i is the speed, with which magnetic lines are entering the current sheet (a reconnection speed) and V_o the speed of the material expelled from the end of the sheet by the enhanced plasma pressure (a magnetic field discharge).

[50] Therefore, if one can measure the both components of magnetic field (B_i and B_o) as well as the speed of expulsion V_o then this would define the speed of magnetic line reconnection V_i. It is difficult to catch the changes of the magnetic field B_i in a current sheet itself because of its small size. However, by measuring magnetic field in the foot points associated with the reconnecting loops one can get the magnetic field variations during a reconnection in half of the loop.

[51] It has to be noted that in real flaring events there are often more than 4 magnetic sources and two interacting flux tubes involved in a reconnection process that results in more complicated QSL shapes and in a several stage reconnection processes. For evaluation purposes one can use "quasi-independent magnetic sources" by considering in the first approach only the closest magnetic sources and assuming that they form a minidiffusion region where the reconnection occurs. In the second approach, the further apart set of the sources can be included and so on. In this way, the reconnection initiated by complicated sources is reduced to the classic global reconnection model for 4 closest sources described above that can now be applied to the measurements of magnetic field changes in the whole region reported above.

[52] In the considered event, as we have pointed out in section 3.4, the outgoing speed V_o of the magnetic discharge in this particular flare can be traced from the projection of this discharge onto the apparent neutral magnetic line, i.e., the speed V_o, with which the material is expelled from the end of the currents sheet according to the global reconnec-
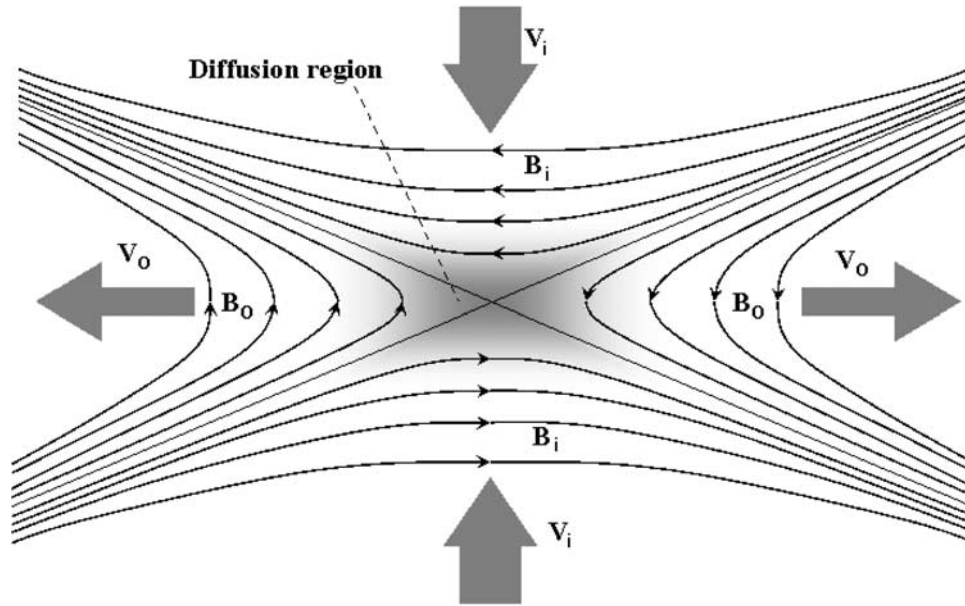
Figure 12. The schematic presentation of a magnetic reconnection region located in the separator with B_i and B_o are incoming and outgoing magnetic field which enter the diffusion region with the speeds V_i and V_o, respectively [from *Priest*, 1984].

tion models [*Titov and Hornig*, 2002]. Hence in this particular magnetic topology and projection onto the flat solar magnetogram image $V_o \simeq V_{anl}$ that is assumed to be the same for the magnetic field changes in the whole area and in the sources associated with HXR sources (see section 3.1 and section 3.3). The energy release rate $\frac{dE}{dt}$ during a flare is the product of the Poynting flux into the reconnection region S and the area of this region A_{rec}, i.e., $\frac{dE}{dt} = S \times A_{rec}$. The Poynting flux, or magnetic energy flux per a given area A and a time t, can be estimated as follows [*Priest*, 1984]:

$$S \equiv \frac{dE}{dtdA} \cong 2 \times \frac{B_c^2}{8\pi} \times V_i \qquad (2)$$

where E is the energy stored in the magnetic field, B_c is the magnetic induction in the corona where the reconnection occurs (which is B_i in the current model from Figure 5), V_i is the velocity of internal magnetic flows, or the reconnection speed and the factor 2 takes into account the flux from both polarities. Since magnetic field strength in the corona is rather difficult to measure, one needs to refer to the magnetic field measurements in the photosphere using the magnetic flux conservation law (for details, see *Priest* [1984]):

$$B_c \times A_c \approx B_{phot} \times A_{ph} \qquad (3)$$

where B_{phot} is the photospheric magnetic field in the foot points corresponding to the QSL trace of the loop participating in the reconnection process and A_c and A_{ph} are the flux tube areas in the corona and photosphere, respectively. Therefore the coronal magnetic field B_c can be evaluated from formula (3) with the assumption that the ratio $A_{ph}/A_c \approx \alpha$, where α is a constant from the

force-free approach of magnetic field extrapolation [*Priest*, 1984]:

$$B_c \simeq \alpha \times B_{phot} \approx 0.2 \times B_{phot} \qquad (4)$$

Then by substituting formula (4) for B_o the changing coronal magnetic field B_c and taking into account the comments after the formula (1), the reconnection rate (1) can be re-written as follows:

$$B_i \times V_i \simeq \alpha \times B_{phot} \times V_{anl} \qquad (5)$$

[53] Taking into account the photospheric magnetic field extrapolation into the corona by formula (4) and the equation (1) for the reconnection rate, the Poynting vector can be calculated as follows:

$$S = \frac{1}{4\pi} B_c \times B_c \times V_i = \frac{\alpha}{4\pi} \times B_{phot} \times B_{phot} \times V_{anl}. \qquad (6)$$

The reconnection area A_{rec} is unknown since we do not know the height where the process of reconnection takes place. However, one can estimate its lowest limit from the area A_{ph} of the photospheric foot point involved in the magnetic field irreversible changes as $A_{rec} \simeq A_{ph}$ which can be increased by $1/\alpha$ in the current assumption, if the reconnection takes place on the loop top in corona. Then the lowest estimation of the energy release rate can be calculated by multiplying the Poynting flux over the area involved in the reconnection process, and the total energy can be estimated by multiplying the energy rate by the time when the magnetic changes occur, i.e., the time of ANL movement in the current measurements.

[54] Therefore, by measuring a LOS magnetic field B_{phot} in the foot point of a reconnecting loop, its area A_{ph} and the

speed of expulsion V_{anl}, one can estimate a reconnection speed (5), Poynting flux (6) and the energy release rate during the reconnection of magnetic field in the interacting foot points (photospheric sources).

[55] With the LOS measurements an absolute value of the released energy can be underestimated by the factor of $1/\cos(\theta)/\cos(\phi)$ owing to its dependence on the flare location on the solar disk where θ is a heliolatitude and ϕ is a heliolongitude. During reconnection the position of the apparent neutral line on the photosphere is defined by the magnetic field squashing caused by the position of photospheric sources and their movements [Titov et al., 2002]. A tilt of reconnecting loops in the corona is not expected to change the photospheric source location and their large magnitude (a few hundred Gauss) in comparison with the weak background magnetic field (20 G and lower). However, a magnetic field tilt can change the positions of QSLs and a separator in the imaginary hemispheres connecting these sources (Figure 11) that can lead to the tilt deduced from the γ ray sources [Share et al., 2003].

4.2. Magnetic Reconnection Rate

[56] Let us evaluate the reconnection rate and Poynting flux of the magnetic reconnection as observed from the whole area (Figures 5–7) and from the source D (Figure 8, top).

[57] The total magnetic field variations (Figure 7, bottom) occur for approximately 5.8 min (348 s), and the magnetic flux for the area covered by the central mask changes by 3.3×10^{20} Mx or 1.2×10^{21} Mx taking into account the projection effect by dividing by $\cos(\phi)$ where (ϕ) is a heliolongitude $(\phi) \simeq 74° \Rightarrow 1/\cos(\phi) = 3.6$. This will result in a reconnection speed of about 3.1×10^{18} Mx/s. The magnetic variations from the whole rectangular area (see Figures 5 and 6) were 1.1×10^{21} Mx which lasted for ∼6 min resulting in the reconnection speed of 3.0×10^{18} Mx/s.

[58] For comparison we calculated the magnetic dissipation rate using the measured magnetic field changes in the source D. The area covered by the D source was about 10×10 arcsec^2 giving us $10^2 \times (750)^2 \times 10^{10}$ cm$^2 = 5.6 \times 10^{17}$ cm^2, that can be increased to 2×10^{18} cm^2 because of the projection effect on a solar disk.

[59] The negative magnetic field increased (in absolute value) by ~ -120 G (from -320 G to -440 G) during 2 min (120 s) (Figure 8, top). This produces a magnetic flux change of $120 \times 2 \times 10^{18} \simeq 2.4 \times 10^{20}$ Mx. Hence the reconnection rate in this foot point is $2.4 \times 10^{20}/120$ s $\simeq 2.0 \times 10^{18}$ Mx/s being rather close to those of $\simeq 3.1 \times 10^{18}$ Mx/s obtained from the total magnetic field changes above.

[60] Now let us we consider the irreversible magnetic field variations of 100 G occurring from 0029:00 UT for ∼2 min in the source B (-360 G) and the irreversible part of magnetic variations, that was a difference between magnetic field before and after the flare, occurring from 0029:00 UT for 4 min in the source C ($+350$ G). The maximum areas covered by the sources B and C are 1.2×10^{17} cm^2 and 3.2×10^{17} cm^2, respectively, which are increased to 4.3×10^{17} cm^2 and 1.2×10^{18} cm^2 by the projection effect. This will result in flux changes of 4.3×10^{19} Mx for the source B and 1.2×10^{20} Mx for the source C leading to a reconnection rate of 3.6×10^{17} Mx/s in the source B and 5.0×10^{17} Mx/s in the source C.

[61] The neutral line variations occurred for 2 min from 0026 UT (see section 3.4), which suggests that the duration of reconnection in these sources was not less then 120 s. However, the magnetic changes measured in Figures 5–7 indicate that these changes have longer duration, up to 10 min, with, possibly, a slower rate. The estimations of the maximum Poynting vector from formula (5) in the source D with an average magnetic field of -380 G and the speed of magnetic changes corresponding to the ANL speed (250 km/s in Figure 10) result in about 1.1×10^{12} erg · cm^{-2}s^{-1} for 2 min duration or even by factor 5 higher for the full time of 10 min. Since we have measured the ANL linear increase during 1 min with a following linear decrease for another minute, the average Poynting flux (see formula (5) also has a triangle temporal profile that results in an average Poynting flux of about half its maximum value, i.e., 5.5×10^{11} erg · cm^{-2}s^{-1}, or $\sim 2.5 \times 10^{12}$ erg · cm^{-2}s^{-1} for the whole time of magnetic changes.

[62] In turn, taking into account the area of the source D this results in a magnetic energy release rate of about 1.1×10^{29} erg/s and the part of the total energy released in this process during 120 s is about 1.3×10^{31} erg. If one adds the absolute magnetic field increase by 100 G with the relevant sign occurred in the sources B (-360 G) and C ($+350$ G) (see section 3.3), respectively, the total released energy can be increased up to 2.3×10^{31} erg. Although only the LOS magnetic field was used for the measurements of the released energy in the magnetic sources and the reconnection time of 2 min instead of 10 registered from the magnetic field changes, this estimation is in a good agreement with the energy 1.0×10^{31} erg deduced from the nonthermal emission in this flare [Holman et al., 2003; Emslie, 2003]. This magnitude can easily be increased by factor 5 to $\sim 1.0 \times 10^{32}$ erg, if the whole period of magnetic changes are taken into account, which confirms that the irreversible magnetic changes occurring prior to the first hard X-ray maximum in the sources D, B and C, can provide enough energy to account for the observed hard X-ray emission.

[63] The reconnection rate and energy released in this flare measured from the LOS magnetic field in the whole area and in the 3 observed HXR sources are sufficient to account for the HXR energetics in the flare while there were no significant magnetic field changes measured after the first HXR maximum. This can support the suggestion that the primary reconnection process is associated with the HXR sites and the secondary one occurs above these sites higher or around the source A in the higher loops. This scenario is in agreement with the phenomenological tether-cutting model proposed by Yurchyshyn et al. [2004] from the movement investigation of the HXR sources.

[64] Now we would like to discuss further the measurements of HXR and γ ray emission in this two stage reconnection process and extend the phenomenological scenario of particle acceleration occurring in this flare proposed by Yurchyshyn et al. [2004]. The main acceleration is suggested to be caused by an electric field in the nonneutral reconnecting current sheets occurring during the primary reconnection in the lower system of loops above the foot points (possibly, source A) connected to the other HXR sources (B–D) producing power law electron and proton beams which are fully or partially separated

[*Zharkova and Gordovskyy*, 2004, 2005] (hereinafter referred to as ZG04 and ZG05, respectively) and precipitate into the opposite foot points of reconnecting loops. Because there were no accelerated particles observed from this flare [*Gopalswamy et al.*, 2003], the reconnection has to occur in the closed loop systems embedded into the photosphere and associated with the HXR sources B, C and D.

[65] Electron beams precipitate either into the thin target (sources D) or thick target (sources B and C) atmospheres, that produces the first observed HXR increase. These electrons can be further accelerated stochastically on the waves induced by these beams in a dense flaring atmosphere of the foot points resulting in the later HXR emission increase in the same sources. However, it is not clear yet where the protons precipitate since, obviously, their paths in the first acceleration were obscured by the loops with electrons because of a smaller scale of the lower loop system. Alternatively, they may produce the H_α emission enhancement in the third loop across the ANL as discussed in section 2.2 that appears after the main HXR maximum and minutes later after the two ribbon loops brightened.

[66] The secondary (and weaker) reconnection process occurring in the larger magnetic loops above the lower loop system is also likely to produce much weaker but still separated electron and proton beams. The separation of electrons from protons in a nonneutral current sheet located in the southern end of the loop leads to a longer traveling time by the protons because of their smaller velocities gained at the acceleration (a factor of 10^6 cm/s for protons and up to 10^8 cm/s for electrons, ZG04). Then the spatial separation of the γ ray source from the HXR source and its time delay to HXR of about 10 s [*Smith et al.*, 2003] can be easily explained by this separation and a location of the secondary acceleration site closer to the southern foot point where the γ source is seen. However, the available data is not sufficient to make quantitative simulations of the possible acceleration scenarios that will require more multiwavelength observations of similar events in the future.

5. Conclusions

[67] In the present paper we have studied the two types of LOS magnetic field variations associated with the 23 July 2002 flare: the reversible, or transient type, ones and the irreversible ones. The former was previously concluded to be induced by nonthermal excitation of Ni atom by electron beams [*Zharkova and Kosovichev*, 2002], the latter are related to the magnetic field dissipation in the vicinity of the apparent magnetic neutral line.

[68] 1. Prior to the flare there are 9 preexisting sources of strong magnetic field of both positive and negative polarities about 400–600 G. There are also 6 new negative sources: 2 negative of −580 G and −380 G and 4 positive of about 100–160 G appeared in the future locations of the hard X-ray sources B and C in a close location to the apparent neutral biggest curvature (bump) toward the negative polarity just 2 min prior the flare hard X-ray maximum.

[69] 2. These new sources are associated with the magnetic discharge, or expulsion, appeared during a magnetic reconnection that fits well the phenomenological tether-cutting reconnection model suggested by *Yurchyshyn et al.* [2004]. This results in a fast movement with a speed about 250 km/s of the apparent neutral line (ANL) toward the positive polarity that occurs 2 min prior to the maximum of the first hard X-ray burst at 0028:00 UT. This discharge can initiate another reconnection process in the upper loops that results in another magnetic flux eruption and ANL movement occurred at 0033:00 UT when the secondary HXR maximum is observed.

[70] 3. The cross correlation of the temporal variations of magnetic field with the hard X-ray light curves in the 0.3–2 MeV energy band shows the maximum correlation coefficient of 0.6 2 min prior to the HXR flare onset, tha drops down immediately after the first HXR maximum. The lower energy 12–25 keV band shows the maximum correlation coefficient of 0.5 1 min before the flare start and it lasts for 10 min to the first HXR maximum (0029:00 UT) and beyond.

[71] 4. The magnetic flux in the whole area associated with the flare covered by the large rectangular mask was found to change by 1.1×10^{21} Mx during 6.0 min at the rate of 3.0×10^{18} Mx/s. From the smaller area covered by the central mask around the ANL the magnetic flux changes were $\sim 3.5 \times 10^{20}$ Mx during 5.8 min at the rate of 3.2×10^{18} Mx/s.

[72] 5. In the hard X-ray source D a magnetic flux change of 2.4×10^{20} Mx occurred prior to the first hard X-ray maximum and it was associated with the irreversible increase by ~ -120 G of the magnetic field of negative polarity that occurred for 2 min prior the first HXR maximum. This resulted in the reconnection rate of $\sim 2 \times 10^{18}$ Mx/s that is comparable with those deduced from the total LOS magnetic field variations above confirming magnetic energy dissipation in this source. From 0028:00 UT but prior to the second hard X-ray maximum, these magnetic flux changes were followed by those of the source B $(4.3 \times 10^{19}$ Mx) and the source C $(1.2 \times 10^{20}$ Mx) leading to a reconnection rate of 3.6×10^{17} Mx/s in the source B and 5.0×10^{17} Mx/s in the source C. The source C with positive magnetic field also shows reversible changes on top of the irreversible ones reflecting a substantial presence of high-energy electrons causing the line intensity increase in this foot point.

[73] 6. The average Poynting vector from the source D, measured from an increase of the LOS magnetic field absolute magnitude from −300 G to −410 G, is estimated to be $\sim 5.5 \times 10^{11}$ erg $\times$ cm^{-2}s^{-1} for the 2 min period when only the ANL movement is registered or up to $\sim 2.5 \times 10^{12}$ erg $\cdot$ cm^{-2}s^{-1} for the whole period of magnetic changes.

[74] 7. The average energy release rate associated with the source D was estimated to be about 5×10^{29} erg/s and the total energy released in this foot point during the 2 min of the neutral line movement was about 1.2×10^{31} erg while the total energy released during the 10 min of the registered magnetic changes from the whole area including the sources B, C and D was about 1.0×10^{32} erg.

[75] We propose to explain the spatial separation of the γ ray source from HXR sources and their time delay of about 10 s by the separation of power law electron and proton beams [*Zharkova and Gordovskyy*, 2004, 2005] at ejection from the secondary reconnecting site occurring in the upper loops above the HXR source A that is initiated by the

emerging flux from the first reconnection in the lower loops associated with the HXR sources B, C and D.

References

Amari, T., J. F. Luciani, Z. Mikic, and J. Linker (2000), A twisted flux rope model for coronal mass ejections and two-ribbon flares, *Astrophys. J.*, *529*, L49.

Antiochos, S. K., C. R. DeVore, and J. A. Klimchuk (1999), A model for solar coronal mass ejections, *Astrophys. J.*, *510*, 485.

Cameron, R., and N. Sammis (1999), Tangential field changes in the great flare of 1990 May 24, *Astrophys. J.*, *525*, L61.

Canfield, R. C., H. S. Hudson, and D. E. McKenzie (1999), Sigmoidal morphology and eruptive solar activity, *Geophys. Res. Lett.*, *26*, 627.

Demoulin, P., L. G. Bagala, C. H. Mandrini, J. C. Henoux, and M. G. Rovira (1997), Quasi-separatrix layers in solar flares: II. Observed magnetic configurations, *Astron. Astrophys.*, *325*, 305.

Emslie, A. G. (2003), The determination of the total injected power in solar flare electrons, *Astrophys. J.*, *595*, L119.

Firstova, N. M., Z. Xu, and C. Fang (2003), H-alpha line polarization in the major flare of 2002 July 23: I. Observations and data analysis, *Astrophys. J.*, *595*, L131.

Fisher, G. H., R. C. Canfield, and A. N. McClymont (1985), Flare loop radiative hydrodynamics: V. Response to thick-target heating; VI. Chromospheric evaporation due to heating by nonthermal electrons; VII. Dynamics of the thick-target heated chromosphere, *Astrophys. J.*, *289*, 414.

Forbes, T. G., and P. A. Isenberg (1991), A catastrophe mechanism for coronal mass ejections, *Astrophys. J.*, *373*, 294.

Gopalswamy, N., B. R. Dennis, M. L. Kaiser, S. Krucker, R. P. Lin, and A. Vourlidas (2003), Why was there no solar energetic particle event associated with the gamma-ray line flare of 2002 July 23?, paper presented at the American Astronomical Society/SPD Meeting 34, Abstract 22.02, Greenbelt, Md., June.

Gorbachev, V. S., and B. V. Somov (1988), Photospheric vortex flows as a cause for two-ribbon flares: A topological model, *Sol. Phys.*, *117*, 77.

Handy, B. N., et al. (1999), The transition region and coronal explorer, *Sol. Phys.*, *187*, 229.

Holman, G. D., L. Sui, R. A. Schwartz, and A. G. Emslie (2003), Electron Bremsstrahlung hard X-ray spectra, electron distributions, and energetics in the 2002 July 23 solar flare, *Astrophys. J.*, *595*, L103.

Isobe, H., T. Yokoyama, M. Shimojo, T. Marimoto, H. Kozu, S. Eto, N. Narukage, and K. Shibata (2002), Reconnection rate in the decay phase of a long duration event flare on 1997 May 12, *Astrophys. J.*, *566*, 528.

Karlicky, M., and J. C. Henoux (2002), Impact H-alpha line polarization and return current, *Astron. Astrophys.*, *383*, 713.

Kosovichev, A. G., and V. V. Zharkova (2001), Magnetic energy release and transients in the solar flare of 2000 July 14, *Astrophys. J.*, *550*, L155.

Krucker, S., G. J. Hurford, and R. P. Lin (2002), Hard X-ray source motions in the 2002 July 23 gamma-ray flare, *Astrophys. J.*, *595*, L103.

Lin, R. P., et al. (2002), The Reuven Ramaty high-energy solar spectroscopic imager (RHESSI), *Sol. Phys.*, *210*, 3.

Lin, R. P., et al. (2003), RHESSI observations of particle acceleration and energy release in an intense solar gamma-ray line flare, *Astrophys. J.*, *595*, L69.

Liu, Y., Y. Jaing, H. Ji, H. Zang, and H. Wang (2003), Observational evidence of a magnetic flux rope eruption associated with X3 flare on 2002 July 15, *Astrophys. J.*, *593*, L137.

Longcope, D. W., and H. R. Strauss (1994), The form of ideal current layers in line-tied magnetic fields, *Astrophys. J.*, *437*, 851.

Mandrini, C. H., P. Demoulin, M. J. Rovira, J. de La Beaujardiere, and J. C. Henoux (1995), Constraints on flare models set by the active region magnetic topology of AR 6233, *Astron. Astrophys.*, *303*, 927.

Moore, R. L., and B. J. LaBonte (1980), The filament eruption in the 3B flare of July 29, 1973: Onset and magnetic field configuration, in *IAU Symposium 91: Solar and Interplanetary Dynamics*, edited by M. Dryer and E. Tandberg-Hanssen, p. 207, Springer, New York.

Moore, R. L., G. J. Hurford, H. P. Jones, and S. R. Kane (1984), Magnetic changes observed in a solar flare, *Astrophys. J.*, *276*, 379.

Patterson, A. (1984), Flares in Hale 17760: Magnetic transients in the 1981 July 27 flare, *Astrophys. J.*, *280*, 884.

Patterson, A., and H. Zirin (1981), Transient magnetic field changes in flares, *Astrophys. J.*, *243*, L99.

Priest, E. R. (1984), *Solar Magneto-Hydrodynamics*, *Geophys. Astrophys. Monogr. Ser.*, Springer, New York.

Priest, E. R., and P. Demoulin (1995), Three-dimensional magnetic reconnection without null points: 1. Basic theory of magnetic flipping, *J. Geophys. Res.*, *100*, 23,443.

Priest, E. R., and T. Forbes (2000), *Magnetic Reconnection*, Cambridge Univ. Press, New York.

Scherrer, P. H., et al. (1995), The solar oscillations investigation: Michelson Doppler imager, *Sol. Phys.*, *162*, 129.

Share, G. H., R. J. Murphy, D. M. Smith, R. P. Lin, B. R. Dennis, and R. A. Schwartz (2003), Directionality of flare-accelerated alpha-particles at the Sun, *Astrophys. J.*, *595*, L89.

Smith, D. M., et al. (2002), The RHESSI spectrometer, *Sol. Phys.*, *210*, 33.

Smith, D. M., G. H. Share, R. J. Murphy, R. A. Schwartz, A. Y. Shih, and R. P. Lin (2003), High-resolution spectroscopy of gamma-ray lines from the X-class solar flare of 2002 July 23, *Astrophys. J.*, *595*, L81.

Somov, B. V. (2000), *Cosmic Plasma Physics*, *Astrophys. Space Sci. Libr.*, vol. 251, Springer, New York.

Somov, B. V., B. J. Semulinja, and A. R. Spektor (1982), Hydrodynamic response of the solar chromosphere to an elementary flare burst: II. Thermal model, *Sol. Phys.*, *81*, 281.

Sterling, A. C., R. L. Moore, J. Qui, and H. Wang (2001), H-alpha proxies for EIT crinkles: Further evidence for preflare "breakout"-type activity in an ejective solar eruption, *Astrophys. J.*, *561*, 1116.

Sweet, P. A. (1969), Mechanisms of solar flares, *Annu. Rev. Astron. Astrophys.*, *7*, 149.

Titov, V. S., and G. Hornig (2002), Magnetic connectivity of coronal fields: Geometrical versus topological description, *Adv. Space Res.*, *29*(7), 1087.

Titov, V. S., P. Demoulin, and G. Hornig (1999), Quasi-separatrix layers: Refined theory and its application to solar flares, in *Magnetic Fields and Solar Processes: The 9th European Meeting on Solar Physics*, edited by A. Wilson, *Eur. Space Agency Spec. Publ., ESA SP-448*, 715.

Titov, V. S., G. Hornig, and P. Demoulin (2002), Theory of magnetic connectivity in the solar corona, *J. Geophys. Res.*, *107*(A8), 1164, doi:10.1029/2001JA000278.

Wang, H., M. W. Ewell, H. Zirin, and G. Ai (1994), Vector magnetic field changes associated with X-class flares, *Astrophys. J.*, *424*, 436.

Wang, H., T. J. Spirock, J. Qui, H.-S. Ji, V. Yurchyshyn, Y.-J. Moon, C. Denker, and P. R. Goode (2002), Rapid changes of magnetic fields associated with six X-class flares, *Astrophys. J.*, *576*, 497.

Yurchyshyn, V., H. Wang, V. Abramenko, T. J. Spirock, and S. Krucker (2004), Magnetic field, H_α and RHESSI observations of the 2002 July 23 gamma-ray flare, *Astrophys. J.*, *605*, 546.

Zarro, D. M., R. C. Canfield, N. Nitta, D. C. Myers, S. E. Gregory, J. Qiu, D. Alexander, H. S. Hudson, B. J. Thompson, and B. J. LaBonte (2000), Max millennium/whole Sun month observations of a sigmoid region (AR 8668), *Bull. Am. Astron. Soc.*, *32*, 817.

Zharkova, V. V., and M. Gordovskyy (2004), Particle acceleration asymmetry in a reconnecting nonneutral current sheet, *Astrophys. J.*, *604*, 550.

Zharkova, V. V., and M. Gordovskyy (2005), Energy spectra of particles accelerated in a reconnecting current sheet with the guiding magnetic field, *Mon. Not. R. Astron. Soc.*, *356*(N3), 1107.

Zharkova, V. V., and V. A. Kobylinsky (1993), The effect of non-thermal excitation and ionization on the hydrogen emission in impulsive solar flares, *Sol. Phys.*, *143*, 259.

Zharkova, V. V., and A. G. Kosovichev (2002), Is Ni I 676.8 nm line affected by electron beams in flaring atmospheres?, in *10th ESPM Proceedings, ESA SP-506*, vol. 2, 1031.

Zharkova, V. V., and D. V. Syniavskii (2000), H-alpha-line impact polarisation by electron beams in solar flares, *Astron. Astrophys.*, *354*, 714.

Zirin, H., and K. Tanaka (1981), Magnetic transients in flares, *Astrophys. J.*, *259*, 791.

_____

A. K. Benkhalil, S. S. Ipson, S. I. Zharkov, and V. V. Zharkova, Department of Cybernetics and Virtual Systems, University of Bradford, Bradford BD7 1DP, UK. (a.k.benkhalil@brad.ac.uk; s.s.ipson@brad.ac.uk; s.zharkov@brad.ac.uk; v.v.zharkova@brad.ac.uk)